Modified Gas-Translation Model for Prediction of Gas Permeation Through Microporous Organosilica Membranes

Hiroki Nagasawa, Takuya Niimi, Masakoto Kanezashi, Tomohisa Yoshioka, and Toshinori Tsuru
Dept. of Chemical Engineering, Hiroshima University, Higashi-Hiroshima, Hiroshima 739–8527, Japan

DOI 10.1002/aic.14578
Published online August 25, 2014 in Wiley Online Library (wileyonlinelibrary.com)

A modified gas-translation (GT) model was applied for the theoretical analysis of gas permeation through microporous organosilica membranes derived from bis(triethoxysilyl)ethane (BTESE) via a sol–gel method using different water/alkoxide molar ratios. The pore sizes of BTESE-derived membranes were quantitatively determined by normalized Knudsen-based permeance analysis, which was based on a modified-GT model, using experimentally obtained permeances of He, H_2, N_2, C_3H_8, and SF_6. The pore sizes of BTESE-derived membranes were successfully controlled from 0.65 to 0.46 nm by increasing the H_2O/BTESE ratio from 6 to 240. Furthermore, theoretical correlations of all possible pairs of permeance ratios were calculated based on the modified-GT model. The experimental data were in good agreement with the theoretical correlation curves, indicating that the modified-GT model can clearly explain gas permeation mechanisms through microporous membranes, and, thus, can be used to predict the gas permeation properties for these membranes. © 2014 American Institute of Chemical Engineers *AIChE J*, 60: 4199–4210, 2014

Keywords: modified gas-translation model, microporous organosilica membranes, bis(triethoxysilyl)ethane, normalized Knudsen-based permeance, gas permeation characteristics

Introduction

Microporous ceramic membranes have received a great deal of attention owing to their potential applications in molecular separation as well as to their superior chemical and thermal stability, which allows these membranes to be operated in a wide variety of separation tasks even under harsh environments. Molecular separation through the microporous ceramic membranes is primarily accomplished by molecular sieving, although the effect of the interaction affinities of guest molecules to the membrane matrix should also be considered. It is, therefore, particularly important to control the size of the micropores because the size of the pores governs the accessibility of the guest molecules into the pores as well as defines the adsorptive properties of the membrane matrix, which consequently determines the separation performance of a given membrane.

Silica is one of the most widely used materials for microporous ceramic membranes because of its amorphous structure,[1,2] which consists of siloxane-based networks with extremely small pores of approximately 0.3 nm, through which only small molecules such as helium and hydrogen can permeate.[3] Thus, amorphous silica membranes, which are typically fabricated by sol–gel[4,5] or chemical vapor deposition (CVD) techniques[6,7] using tetraethoxysilane (TEOS) as a precursor, are known to have good hydrogen permselectivity, owing to the small pore openings formed by siloxane bond networks, and have been extensively investigated for hydrogen separation from gaseous mixtures such as H_2/CO_2, H_2/N_2, and H_2/CH_4. However, the sizes of the micropores for these silica membranes appeared to be too small to achieve an efficient separation of, for example, CO_2/N_2 and CO_2/CH_4, as well as hydrogen separation from light hydrocarbons such as C2—C4. Therefore, the design and control of the microporous structures is quite important for the implementation of amorphous silica membranes.

The organic-template method is one of the most accepted methods for the pore-size tuning of amorphous silica membranes.[8] When using the organic-template method, the pore sizes can be controlled by burning out the organic functional groups during the postsynthesis treatment. Therefore, the size and shape of the micropores in the membranes will be determined by the size and shape of the organic functional groups.

Another promising method, reported more recently in the literature, is the spacer method that uses bridged bis-silyl precursors for the fabrication of microporous organosilica membranes.[9,10] This method can provide a variety of structures by introducing spacers into the normal silica networks. In our previous work, we successfully prepared organosilica membranes via the sol–gel processing of bis(triethoxysilyl)-ethane (BTESE), which is a bis-silyl type alkoxide precursor with ethane groups between the Si atoms.[11] The BTESE-derived membranes showed a significantly high H_2 permeance compared with the previously reported TEOS-derived silica membranes, and possessed a high H_2/SF_6 permeance ratio but a low selectivity for H_2/N_2, suggesting that the diameters of micropores in BTESE-derived membranes were successfully enlarged compared with those in conventional TEOS-derived silica membranes. The pore size of BTESE-

Correspondence concerning this article should be addressed to T. Tsuru at tsuru@hiroshima-u.ac.jp.

derived membranes was estimated to be approximately 0.5 nm.[11] Furthermore, in our most recent work, we examined the effect of water to BTESE molar ratio during the sol preparation on gas permeation properties, and found that the permselectivities through the BTESE-derived membranes were highly dependent on the H_2O/BTESE ratios.[12] According to the single gas permeation results, a higher H_2O/BTESE ratio led to a higher permeance ratio for both H_2/N_2 and H_2/SF_6. In general, the higher water to alkoxide ratios during the hydrolysis and condensation reaction of silicon alkoxides leads to a higher degree of hydrolysis, and results in the formation of sols with a highly cross-linked network structure.[13] In regard to gas separation, a highly cross-linked network structure may provide a microporous membrane with better molecular sieving characteristics. Our results seem to be consistent with this general picture of sol–gel processing, which suggests that a change in the H_2O/BTESE ratio could also provide an opportunity to control the size of the micropores in BTESE-derived membranes.

To design a porous structure of organosilica membranes that could achieve the desired separation, an understanding of the transport mechanism through the micropores is essential. The gas transport mechanism through the micropores, whose pore size approaches the size of permeating molecules, can be described theoretically using various models such as the gas-translation (GT) model or the activated Knudsen diffusion, which was originally proposed by Xiao and Wei,[14] as well as by Shelekhin et al.[15] In this model, the permeating molecules are assumed to be restricted in their movement due to the effect from the potential field of the pore wall, and thus, they must overcome certain energy barriers in order to permeate through the pores. The model was further modified by considering the size of the permeating molecules as the modified-GT model and applied to the determination of pore sizes by Lee et al.[16] The method proposed for the determination of pore size is referred to as the normalized Knudsen-based permeance (NKP) method.[16,17] NKP is the ratio of an experimentally observed permeance to the ideal Knudsen permeance for each gas expected from the permeance of a standard gas such as He. NKP indicates the degree of permeance decrement from the ideal Knudsen permeance. As the permeation mechanism is dependent on molecular weight and molecular size in the Knudsen and molecular sieving regimes, respectively, the approximate size of membrane pores can be qualitatively estimated based on the molecular size that caused the permeation mechanism to deviate from Knudsen to molecular sieving.[18,19] Conversely, by plotting experimentally obtained NKP against molecular size together with the NKP equation derived from the modified-GT model, the mean pore diameter for gas permeation can be quantitatively estimated.[16,17]

In our previous study, the modified-GT model was validated by using the gas permeation data from zeolite MFI and DDR membranes.[16,17] The NKP-based mean pore diameters were calculated based on the permeation data and the calculated values showed good agreement with the intrinsic pore sizes for the corresponding zeolites. As an extension of this achievement, in the present study, we attempted to apply the modified-GT model to the analysis and prediction of the gas permeation properties of microporous organosilica membranes, which consisted of amorphous network structures. Microporous organosilica membranes were prepared via the hydrolysis and condensation of bis(triethocysilyl)ethane (BTESE). The gas permeation properties of BTESE-derived membranes were determined experimentally and discussed based on the modified-GT model. BTESE membranes were fabricated in a wide range of H_2O/BTESE molar ratios in order to change their network structure, and then the single gas permeances were measured for each membrane. The temperature dependencies of single gas permeances were also measured to establish the dominant permeation mechanisms through the membranes. The pore sizes that were effective for gas permeation were quantitatively evaluated using the NKP method, which was developed based on the modified-GT model. Finally, the gas permeation properties were predicted based on the modified-GT model, and were compared with those obtained from the experimental observations.

Experimental

BTESE (Gelest) was hydrolyzed and condensed to form polymeric sols in ethanol with water and hydrochloric acid. The details of the procedure for sol preparation and membrane fabrication have been described elsewhere.[11,12] First, BTESE was homogeneously dissolved in ethanol, and then a mixture of water, hydrochloric acid, and ethanol was added dropwise to the solutions under vigorous stirring. To investigate the effect of the water/alkoxide ratio during the sol preparation stage, the molar compositions of the BTESE solutions were varied from BTESE:H_2O:HCl = 1:6:0.1 to 1:240:0.1 with the equivalent weight % of BTESE kept at 5.0 wt %. After this addition, the solutions were further stirred for 1 h at room temperature to develop BTESE polymeric sols.

Porous α-alumina tubes (Mitsui Grinding Wheel Co., Japan; porosity: 50%; average pore size: 1 μm; outer diameter: 10 mm) were used as supports for BTESE-derived membranes. First, α-alumina particles (average particle diameter: 0.2, 1.9 μm) were coated on the outer surface of the porous supports using silica-zirconia (Si/Zr = 1/1) colloidal sols as the binder, and the supports were fired at 550°C for 30 min to make the surface smooth. Then, SiO_2-ZrO_2 sols were coated onto the particle layers, which were subsequently fired at 550°C for 15 min. This procedure was repeated several times to form the intermediate layers with a pore size of several nanometers. Finally, BTESE-derived membranes were obtained by coating BTESE polymeric sols onto the intermediate layers, followed by calcination at 300°C in air for 30 min. The coating and calcination procedure was repeated twice to obtain separation layers.

Gas permeation measurements were performed using single components of He, H_2, N_2, C_3H_8, and SF_6. The permeation gas was fed to the outer side of the membrane, while the inner side of the membrane was maintained at atmospheric pressure. The transmembrane pressure was maintained at 0.1–0.2 MPa, and the permeation flow rate was measured using a soap-film flow meter (Horiba Co., Japan). The measurements were performed at 200°C, unless otherwise specified.

Theory

Gas-translation model

The gas permeation through microporous membranes can be accomplished by a combination of Knudsen diffusion, surface diffusion, and molecular sieving mechanisms. Several theoretical models have been proposed to describe the

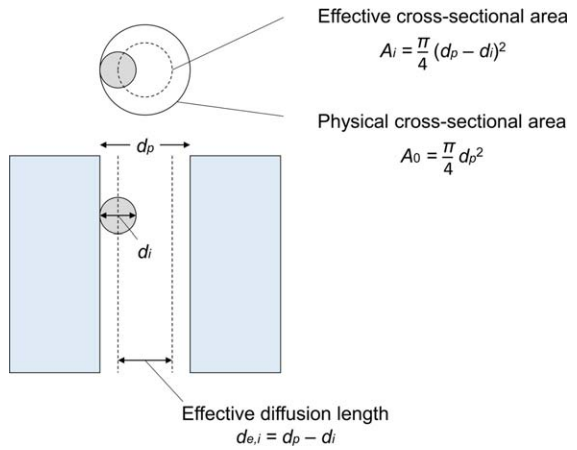

Figure 1. Schematic drawing of the permeation of molecules with a molecular size of d_i through a cylindrical micropore with a pore diameter of d_p.

[Color figure can be viewed in the online issue, which is available at wileyonlinelibrary.com.]

gas permeation properties of microporous membranes. Xiao and Wei first developed a model, which was referred to as the gas-translation (GT) or activated Knudsen diffusion model, to analyze the diffusion of hydrocarbons in zeolites.[14] This model was then extended by Shelekhin et al. to predict the gas permeability in microporous molecular sieve membranes.[15] In the GT model, the permeating molecules keep their gaseous characters but may be restricted in their movements due to the effect from the potential field of the pore wall; thus, they must overcome certain energy barriers to transport through the pores. Using the membrane structural parameters that include the porosity, ε, the tortuosity, τ, and the membrane thickness, L, the permeance for the ith component in the GT model, $P_{GT,i}$, can be given as follows

$$P_{GT,i} = \rho_i \frac{\varepsilon}{\tau L} d_e \sqrt{\frac{8}{\pi M_i RT}} \tag{1}$$

where ρ_i is the probability of diffusion for the ith component, that is, the probability that the gas molecule will move in the direction of permeation, d_e is the effective diffusion length, that is, the average distance between collisions or jumps, M_i is the molecular weight of the ith component, R is the gas constant, and T is the absolute temperature. The porosity, ε, considered here is defined by the membrane area, A_m, the number of pores, N_p, with a mean pore diameter of d_p, and the physical cross-sectional area of the pore, A_0, as follows

$$\varepsilon = \frac{N_p A_0}{A_m} = \frac{N_p \pi d_p^2/4}{A_m} \tag{2}$$

The probability of diffusion, ρ_i, is expressed with the pre-exponential factor, ρ_g, and the activation energy, $E_{P,i}$, to overcome the diffusion barrier[14]

$$\rho_i = \rho_g \exp\left(-\frac{E_{P,i}}{RT}\right) \tag{3}$$

The pre-exponential factor, ρ_g, is the geometrical probability, that is given by, for example, the number of adjustment sites where an activated molecule at a site can jump into,[14] or the cross-sectional area ratio of the neck and the cavity in zeolites.[15] The activation energy, $E_{P,i}$, is dependent on the pore size and on the interactions of permeating molecules with the membrane matrix.[15] Substituting Eq. 3 into Eq. 1 and taking the mean pore diameter, d_p, as the effective diffusion length, the permeance, $P_{GT,i}$, can be rewritten as follows

$$P_{GT,i} = \rho_g \frac{\varepsilon}{\tau L} d_p \sqrt{\frac{8}{\pi M_i RT}} \exp\left(-\frac{E_{P,i}}{RT}\right) \tag{4}$$

As described in Eq. 4, unlike the ideal Knudsen diffusion, the permeance under the gas-translation regime shows an exponential dependency on temperature. It should be noted that in the case of a large pore diameter, $E_{P,i}$ and ρ_g become 0 and 1/3 (indicates the one-dimensional direction of permeation in a three-dimensional (3-D) space without spatial obstruction), respectively, so that we obtain an equation that represents the ideal Knudsen diffusion.

Modified gas-translation model

In the original GT model, the geometrical probability, ρ_g, was decided based only on the physical structure of the membrane matrix. In other words, there was no distinction in the geometrical probabilities for molecules with different kinetic diameters, although a permeating molecule is not a mass point in reality, but has a finite size. Therefore, in our previous study, we developed the modified gas-translation model, which took into account the size of permeating molecules, and confirmed it based on the permeation data of zeolite MFI and DDR membranes which consisted of intrinsic pores.[16,17]

In the modified-GT model, the geometrical probability for the ith component, $\rho_{g,i}$, is given as the product of (1) the ratio of the effective cross-sectional area of a pore for the ith component, A_i, over the physical cross-sectional area of the pore, A_0, and (2) the random factor 1/3 in a 3-D space, as follows

$$\rho_{g,i} = \frac{1}{3}\frac{A_i}{A_0} \tag{5}$$

For simplicity, we assumed that the shapes of the micropores were cylindrical with corresponding diameters, d_p, as shown in Figure 1. As the center of the permeating molecules cannot approach the pore walls, the effective cross-sectional area of a pore, A_i, is supposed to be a circle with a diameter equal to the effective diffusion length, $d_{e,i}$, which can be assumed as follows

$$d_{e,i} = d_p - d_i \tag{6}$$

where d_i is the kinetic diameter of ith component. With these assumptions, Eq. 5 can be recast into the following form

$$\rho_{g,i} = \frac{1}{3}\frac{A_i}{A_0} = \frac{1}{3}\frac{\pi(d_p - d_i)^2/4}{\pi d_p^2/4} = \frac{1}{3}\frac{(d_p - d_i)^2}{d_p^2} \tag{7}$$

Therefore, by introducing Eq. 7 into Eq. 4 and taking the effective diffusion length to be $d_{e,i}$ instead of d_p, the permeance based on the modified-GT model, $P_{m\text{-}GT,i}$, can be determined as follows

$$P_{m-GT,i} = \frac{1}{3}\frac{\varepsilon}{\tau L}(d_p - d_i)\frac{(d_p - d_i)^2}{d_p^2}\sqrt{\frac{8}{\pi M_i RT}}\exp\left(-\frac{E_{P,i}}{RT}\right) \tag{8}$$

$$= \frac{k_{0,i}}{\sqrt{M_i RT}}\exp\left(-\frac{E_{P,i}}{RT}\right) \tag{9}$$

where $k_{0,i}$ is the pre-exponential factor defined by Eq. 10, which can be expressed only by the configuration factors of

membrane (porosity, ε; tortuosity, τ; membrane thickness, L; mean pore diameter, d_p) and a permeating molecule (kinetic diameter, d_i)

$$k_{0,i}=\frac{\varepsilon}{3\tau L}\frac{\left(d_p-d_i\right)^3}{d_p^2}\sqrt{\frac{8}{\pi}} \tag{10}$$

The final formula for the modified-GT model indicates that the permeance is expressed as a function of the cube of the effective diffusion length, together with an inverse square root dependence on both the molecular weight and the absolute temperature and an exponential dependency on the temperature. It should be noted that for the case of $d_i=0$, we obtain an equation of the original GT model, as described in Eq. 4.

The activation energy of permeation, $E_{P,i}$, and the pre-exponential factor, $k_{0,i}$,can be obtained by regression using Eq. 9 with the experimental temperature dependency of the single gas permeance data. It should be noted that $E_{P,i}$ can be interpreted as the sum of the activation energy of diffusion, $E_{D,i}$, for the permeating molecules to overcome the potential barrier, and the energy of interaction, $-\Delta H_i$, on the assumption of a homogeneous potential field inside micropores.[20] For permeation through the small micropores, where the diffusion barrier is a dominant factor for permeation, the apparent activation energy of gases is $E_{p,i}>0$, and is referred to as the activated diffusion. For permeation through the large micropores, where the interaction affinity of permeating molecules with the membrane matrix is more dominant than the geometrical barrier, the apparent activation energy of gases is $E_{p,i}<0$, and is referred to as the surface diffusion. Moreover, for permeation through much larger micropores, where the Knudsen diffusion mechanism becomes dominant, the apparent activation energy of gases is $E_{p,i}=0$. Thus, Eq. 9 covers activated diffusion ($E_{p,i}>0$), surface diffusion ($E_{p,i}<0$), and Knudsen diffusion ($E_{p,i}=0$).

Application of the modified-GT model to gas permeation analysis

An ideal selectivity, $\alpha_{i/j}$, for the ith and jth components can also be estimated from Eq. 8 as the ratio of the permeances

$$\alpha_{i/j}=\frac{P_i}{P_j}=\sqrt{\frac{M_j}{M_i}}\frac{\left(d_p-d_i\right)^3}{\left(d_p-d_j\right)^3}\exp\left(-\frac{E_{P,i}-E_{P,j}}{RT}\right) \tag{11}$$

To simplify the modeling approach, several assumptions were made for Eq. 11.

1. All gas species permeate through an identical size of pore.

2. The difference in activation energy for permeation is negligible, and is independent of gas species, which could be justified for micropores that range from several angstroms to 1 nm.

Accordingly, Eq. 11 can be simplified as follows

$$\alpha_{i/j}=\frac{P_i}{P_j}\approx\sqrt{\frac{M_j}{M_i}}\frac{\left(d_p-d_i\right)^3}{\left(d_p-d_j\right)^3} \tag{12}$$

This equation indicates that an ideal selectivity can be approximately expressed as a function of the mean pore diameter, d_p. Due to the assumptions above, Eq. 12 may not be sufficiently accurate in describing the experimental data where, for example, strong activated or surface diffusion takes place. However, Eq. 12 is of great value in the evaluation of membrane performance because gas selectivity can be quantitatively predicted using the pore size and the size of permeating molecules.

NKP method for pore-size determination

Based on the modified-GT model, we recently proposed the NKP method, which is the simple method for the determination of membrane pore sizes of less than 1 nm.[16,17] NKP, f_{NKP}, is the ratio of the experimentally observed permeance of the ith component divided by the ideal Knudsen permeance of the ith component that can be expected based on the permeance of a standard gas, and given as follows using Eq. 8

$$f_{NKP}=\frac{P_i}{P_S}\sqrt{\frac{M_i}{M_S}}=\frac{\left(d_p-d_i\right)^3}{\left(d_p-d_S\right)^3}\exp\left(-\frac{E_{p,i}-E_{p,S}}{RT}\right) \tag{13}$$

where the subscription "S" represents the standard gas. Helium, which is the smallest gas molecule, would be suitable for the standard gas. It should be noted that in the case of gas permeation by the ideal Knudsen diffusion, $d_S=d_i=0$ and $E_{p,S}=E_{p,i}=0$, f_{NKP} is equal to unity. As f_{NKP} is expressed as a function of the configuration factors and the activation energies, a set of experimental data on the temperature dependency of single gas permeance is needed for the determination of the pore sizes. In our previous studies, in the interest of simplification we applied the assumptions that were made in the previous section to Eq. 13 and obtained the following equation

$$f_{NKP}=\frac{P_i}{P_S}\sqrt{\frac{M_i}{M_S}}\approx\frac{\left(1-\frac{d_i}{d_p}\right)^3}{\left(1-\frac{d_S}{d_p}\right)^3} \tag{14}$$

To estimate the mean effective pore size, d_p, the experimentally obtained f_{NKP} at a permeation temperature of T as a function of the kinetic diameter is best fitted by Eq. 14, using d_p as a fitting parameter. When applying Eq. 14, permeances at the highest possible temperatures are preferred to obtain d_p.[16,17]

Pore-size determination with the temperature dependency of gas permeance

In addition, the mean effective pore size can be more precisely determined using the experimental data on the temperature dependency of single gas permeance.[17] According to Eq. 10, the following relationship can be obtained

$$k_{0,i}=a\left(d_p-d_i\right)^3 \tag{15}$$

where a is a constant that depends only on the structure of the membrane pores and is independent of the permeation molecules, as given by the following

$$a=\frac{\varepsilon}{3\tau L d_p^2}\sqrt{\frac{8}{\pi}} \tag{16}$$

Accordingly, the cubic root of Eq. 15 gives the linear relationship between d_i and $k_{0,i}^{1/3}$ with a slope of $-a^{1/3}$ and an intercept of $-a^{1/3}\,d_p$ as follows

$$\sqrt[3]{k_{0,i}}=\sqrt[3]{a}\mathrm{d_p}-\sqrt[3]{a}\mathrm{d_i} \tag{17}$$

Therefore, from the plot of $k_{0,i}^{1/3}$ against d_i, both the value of d_p as an effective pore size for gas permeation and the structural parameter a can be easily estimated.

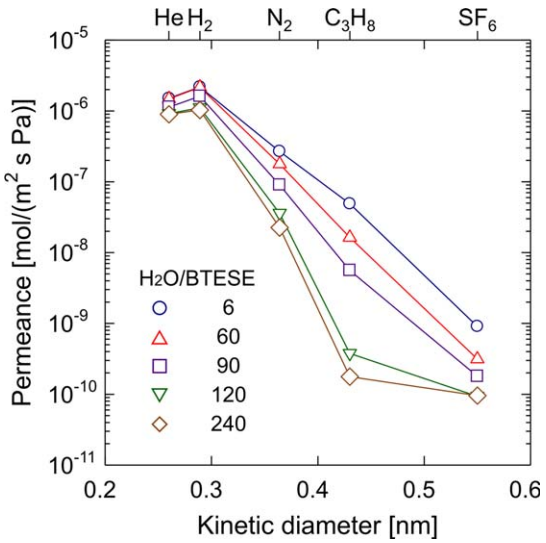

Figure 2. Kinetic diameter dependence of single gas permeance at 200°C for BTESE-derived membranes prepared from sols with different H_2O/BTESE molar ratios.

[Color figure can be viewed in the online issue, which is available at wileyonlinelibrary.com.]

Results and Discussion

Kinetic diameter dependence of gas permeance

Figure 2 shows the kinetic diameter dependence of the single gas permeance at 200°C through BTESE-derived membranes. The BTESE sols used for the top layers were prepared under H_2O/BTESE molar ratios that ranged from 6 to 240. All the membranes tested here showed a high hydrogen permeance on the order of 10^{-6} mol/(m^2 s Pa) at 200°C, together with a permeance ratio of at least 1000 for H_2/SF_6, which was substantially higher than the corresponding Knudsen selectivity of 8.54, suggesting that the BTESE-derived membranes possessed a molecular sieving property. At low H_2O/BTESE ratios, such as H_2O/BTESE = 6 and 60, the membranes showed a moderate selectivity with permeance ratios of 5.62 and 8.31 for He/N_2, and 30.8 and 90.2 for He/C_3H_8, respectively. In contrast, at high H_2O/BTESE ratios such as H_2O/BTESE = 120 and 240, the membranes showed a pronounced selectivity with permeance ratios of 25.5 and 39.7 for He/N_2, and 2420 and 5050 for He/C_3H_8, respectively. According to the kinetic diameter dependence of single gas permeance, the results obviously suggest that the average pore size of the BTESE-derived membranes was decreased with an increase in the H_2O/BTESE ratio.

The effect of the H_2O/BTESE ratio on the gas permeation properties in Figure 2 can be seen more clearly by plotting the single gas permeance and the permeance ratio as a function of the H_2O/BTESE ratio. As is apparent from Figure 3a, the permeance for all types of permeating molecules tended to decrease with an increase in the H_2O/BTESE ratio. The permeance of small molecules such as He (d_i = 0.26 nm) and H_2 (0.289 nm) was, however, only slightly affected by the H_2O/BTESE ratio, as the permeance of He and H_2 only decreased by twofold when the H_2O/BTESE ratio increased from 6 to 240. On the contrary, the permeance of large molecules such as N_2 (0.364 nm), C_3H_8 (0.43 nm), and SF_6 (0.55 nm) decreased more drastically. An abrupt drop in the permeance of N_2, C_3H_8, and SF_6 was observed when the H_2O/BTESE ratios increased from 60 to 120. In particular, the most significant decrease in permeance was observed for C_3H_8. The permeance of C_3H_8 was decreased by more than 100-fold from 4.90×10^{-8} to 1.77×10^{-10} mol/(m^2 s Pa) when the H_2O/BTESE ratio increased from 6 to 240. This result might suggest that, at a higher H_2O/BTESE ratio, the average pore size of BTESE membranes was decreased and approached the size of the C_3H_8 molecules. As a result, as shown in Figure 3b, the permselectivity of small molecules over large ones in BTESE-derived membranes increased significantly as the H_2O/BTESE ratio increased. The relationship between the H_2O/BTESE ratio and pore size will be discussed in detail later. In particular, the BTESE-derived membrane prepared with a H_2O/BTESE ratio of 240 exhibited an outstanding H_2/C_3H_8 and H_2/SF_6 selectivity of 5810 and 10,700, respectively, with a high H_2 permeance of 1.02×10^{-6} mol/(m^2 s Pa).

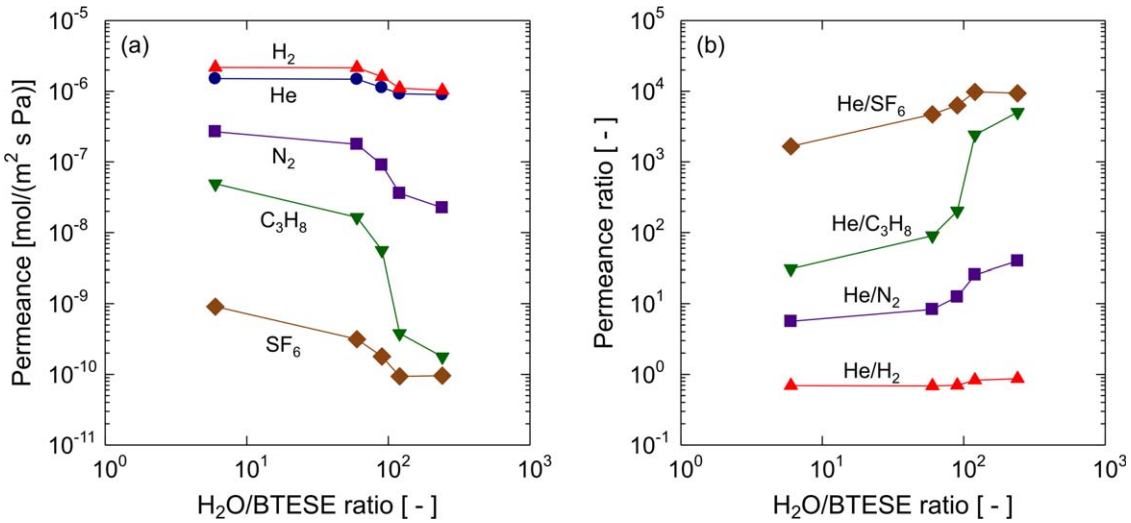

Figure 3. Effect of the H_2O/BTESE molar ratio on (a) single gas permeances and (b) the permeance ratios for BTESE-derived membranes.

[Color figure can be viewed in the online issue, which is available at wileyonlinelibrary.com.]

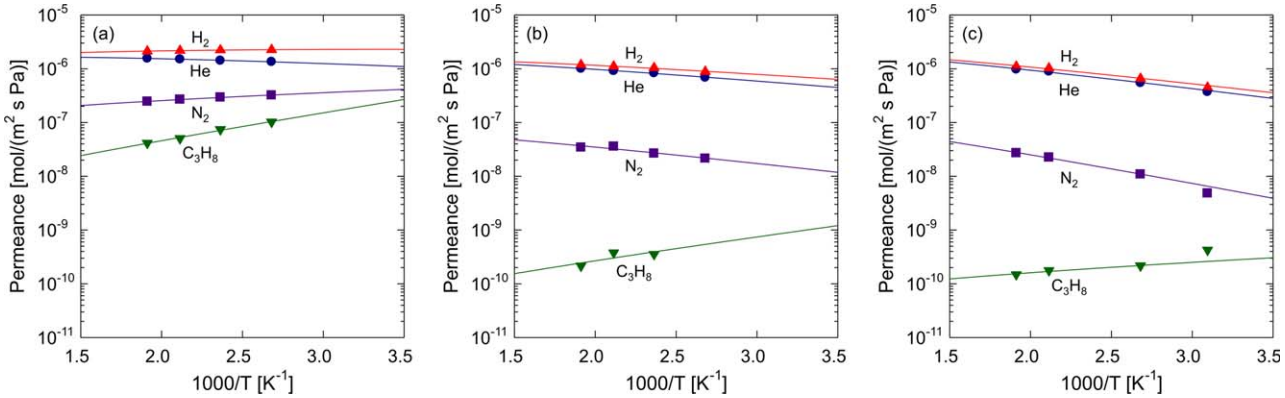

Figure 4. Temperature dependency of single gas permeances for BTESE-derived membranes with (a) H_2O/BTESE molar ratios of 6, (b) 120, and (c) 240.

[Color figure can be viewed in the online issue, which is available at wileyonlinelibrary.com.]

Temperature dependence of gas permeance

The temperature dependence of gas permeance was measured using the same membranes shown in Figure 2. Figure 4a shows the temperature dependence of single gas permeance for BTESE-derived membranes with H_2O/BTESE ratios of 6. The permeance of H_2 slightly decreased with increasing temperature, which can be classified as the Knudsen diffusion mechanism. Meanwhile, the permeance of He increased slightly with increasing temperature, suggesting that a balance of activated and Knudsen permeation mechanisms governed the permeation of He. Due to the near-zero activation energies of He and H_2 permeation, as summarized in Table 1, together with the fact that the He/H_2 permeance ratio remained very close to the ideal Knudsen selectivity of 0.71, the BTESE membrane prepared with a low H_2O/BTESE ratio was thought to have a loose network structure for He and H_2 permeation. The permeance of N_2 decreased with increasing temperature, in the Knudsen-like behavior, with a He/N_2 permeance ratio slightly higher than the ideal Knudsen selectivity, suggesting that the membrane might have relatively large pores that nitrogen molecules could readily permeate through. The permeance of C_3H_8 increased with decreasing temperature, which can be classified as a surface diffusion mechanism, suggesting that C_3H_8 had an attractive interaction with the surface of the membrane pores.

Figures 4b, c show the temperature dependence of single gas permeance for BTESE-derived membranes with H_2O/BTESE ratios of 120 and 240, respectively. For both membranes, the permeances of He, H_2, and N_2 increased with increasing temperature, showing an activated permeation mechanism, whereas that of C_3H_8 increased with a decrease in the temperature, which can be categorized as the surface diffusion mechanism. The He/H_2 permeance ratios for both membranes were slightly higher than that of the ideal Knudsen selectivity, suggesting that the size of the network structure for these membranes were smaller than that for the membrane with a H_2O/BTESE ratio of 6.

The activation energy, $E_{P,i}$, and the pre-exponential factor, $k_{0,i}$, were obtained from Eq. 9 to fit the experimental permeation data. Tables 1 and 2 summarize the activation energies and the membrane structural factors, respectively, for BTESE-derived membranes obtained from the fitting. The activation energies for all types of permeating molecules were higher for the membranes with higher H_2O/BTESE ratios. As, in general, a higher activation energy is required to travel through smaller pores,[21] it can be concluded that the pore size of a BTESE-derived membrane decreased with an increase in the H_2O/BTESE ratio. For all the membranes tested, the pre-exponential factor, $k_{0,i}$, tended to decrease with an increase in the kinetic diameter of the permeating

Table 1. Estimated Values of Activation Energies of Permeation, $E_{p,i}$ (kJ/mol), for BTESE-Derived Membranes

H_2O/BTESE	He	H_2	N_2	C_3H_8
6	3.40	1.18	−1.11	−8.24
120	5.86	4.90	7.53	−6.79
240	8.25	7.65	11.85	−2.01

Table 2. Estimated Values of $k_{0,i}$ for BTESE-Derived Membranes

H_2O/BTESE	He	H_2	N_2	C_3H_8
6	1.42×10^{-5}	8.24×10^{-6}	2.12×10^{-6}	8.53×10^{-8}
120	1.62×10^{-5}	1.09×10^{-5}	2.31×10^{-6}	7.08×10^{-10}
240	2.78×10^{-5}	1.94×10^{-5}	4.67×10^{-6}	1.34×10^{-9}

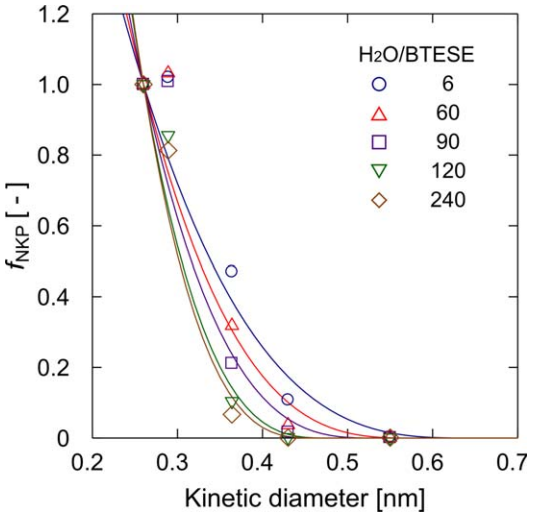

Figure 5. Relationship between kinetic diameters and f_{NKP} at 200°C for BTESE-derived membranes.

Symbols: experimental; solid curves: calculated based on Eq. 14. [Color figure can be viewed in the online issue, which is available at wileyonlinelibrary.com.]

Table 3. Estimated Values of Pore Diameters, d_p (nm) for BTESE-Derived Membranes

H_2O/BTESE	NKP Plot (200°C)	$k_{0,i}^{1/3}$ Plot
6	0.65	0.47
60	0.58	–
90	0.53	–
120	0.48	0.44
240	0.46	0.45

molecules indicating the molecular sieving properties of BTESE-derived membranes.

Pore-size determination by NKP method

Figure 5 shows the plot of f_{NKP} at 200°C for BTESE-derived membranes as a function of the kinetic diameter. The single gas permeation data used are the same as that used in Figure 2. Pore sizes, d_p, were estimated by fitting an experimentally obtained f_{NKP} with Eq. 14. The estimated pore sizes for BTESE-derived membranes showed a tendency to decrease with increase in the H_2O/BTESE ratio. As summarized in Table 3, at low H_2O/BTESE ratios of 6, 60, and 90, the pore sizes were estimated to be 0.65, 0.58, and 0.53 nm, respectively, which were larger than the size of C_3H_8 (0.43 nm). Conversely, at high H_2O/BTESE ratios of 120 and 240, the pore sizes were estimated to be 0.48 and 0.46 nm, respectively, which was much closer to the size of C_3H_8. The pore sizes that were estimated using the NKP method were consistent with the results of the kinetic diameter dependence of single gas permeance (Figure 2), that is, the selectivity of small molecules (He and H_2) over large ones (C_3H_8) in BTESE-derived membranes increased significantly as the H_2O/BTESE ratio increased.

The pore sizes of the BTESE-derived membranes were also determined via the relationship between the value of the cubic root of $k_{0,i}$ (Table 2) and the kinetic diameter of the ith component, d_i, using Eq. 17. As shown in Figure 6, a linear correlation was observed for all membranes and d_p was determined at the intercept of the x axis. The obtained values of d_p are summarized in Table 3 and show a decreasing trend with an increasing H_2O/BTESE ratio, which is consistent with the NKP method.

Pore-size estimation was also conducted for a number of BTESE-derived membranes using the NKP method. The membrane performances and the estimated pore sizes are summarized in Table 4. The membranes shown in Figure 2 are referred to as M(6)-1, M(60)-1, M(90)-1, M(120)-1, and M(240)-1, respectively. Figure 7 shows the relationship between the estimated pore sizes and the H_2O/BTESE molar ratio. As shown here, a strong correlation between H_2O/BTESE and the pore sizes was confirmed. Because the higher water to alkoxide ratios during the hydrolytic condensation reaction led to the formation of a highly cross-linked network, the pore sizes obtained in BTESE-derived membranes showed a decreasing trend along with the H_2O/BTESE ratio. It can be concluded that change in the H_2O/BTESE ratio could control the size of microporous network structures in BTESE-derived membranes.

Comparison of theoretical and experimental gas permeation properties

In Figure 8, the experimental results of the permeance ratios at 200°C for BTESE membranes are plotted as a function of pore size estimated by NKP analysis, and are compared with the theoretical permeance ratios calculated based on the modified-GT model represented in Eq. 12. The symbols denote the experimental results while the solid curves represent the model calculations. The experimental results of the permeance ratios for He/H_2, He/N_2, and He/C_3H_8 show good agreement with the theoretical prediction. The results suggest that, although the pore sizes of BTESE membranes were tuned in a wide range of sizes from 0.45 to 0.9 nm, the selectivity of any given combination of gases can be predicted in a wide range of permeance ratios, 10^0-10^4, if the value of mean pore diameter is given.

In Figure 9, the permeance ratios of He/C_3H_8, H_2/N_2, H_2/C_3H_8, N_2/C_3H_8, and He/SF_6 for BTESE membranes in Table 4 were correlated with the He/N_2 permeance ratio. Experimental results for BTESE membranes at 200°C were compared with the theoretical permeance ratio calculated by Eq. 12. It should be noted that the theoretical curves were calculated using the pore diameter and the kinetic diameters with no fitting parameters. For the correlations of He/C_3H_8, H_2/N_2, H_2/C_3H_8, and N_2/C_3H_8 with He/N_2 (Figures 9a–d), the experimental results agreed surprisingly well with the theoretical curves in a wide range of permeance ratios. For example, as shown in Figure 9a, with increase in the He/N_2 permeance ratio from 2 to 80, the He/C_3H_8 permeance ratio increased from 10 to 10^4 along with the theoretical curve. The membranes with a high H_2O/BTESE molar ratio, which had small pore diameters, are plotted at the top-right of the figure as these membranes possessed high selectivity for both He/N_2 and He/C_3H_8. Conversely, the membranes with a low H_2O/BTESE molar ratio, which had large pore diameters and low selectivity, are plotted at the bottom-left of the figure. The calculated curves accurately predicted the wide range of permeance ratios that were obtained in the gas permeation experiments. This suggested that the permeation of He, H_2, N_2, and C_3H_8 through the BTESE membranes followed the modified-GT model. Moreover, as added in Figures 9a–d, a sol–gel-derived pure silica membrane[22] also agreed well with the theoretical curves, suggesting that gas permeation through the silica membranes occurred in the same manner. It is also worth noting that the results represented here indicate that the permeance ratios for any

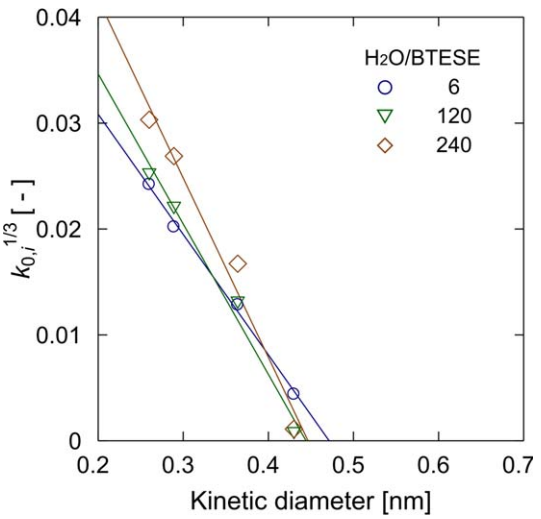

Figure 6. Relationship between kinetic diameters and $k_{0,i}^{1/3}$ for BTESE-derived membranes.

Symbols: experimental; solid curves: calculated based on Eq. 17. [Color figure can be viewed in the online issue, which is available at wileyonlinelibrary.com.]

Table 4. Summary of Gas Permeation Characteristics at 200°C for BTESE-Derived Membranes

No.	H_2O/BTESE	He Permeance (10^{-6} mol/m^2 s Pa)	Permeance Ratio				d_p (nm)
			He/H_2	He/N_2	He/C_3H_8	He/SF_6	
M(6)-1	6	1.51	0.69	5.62	30.8	1,660	0.65
M(6)-2		1.31	0.70	4.83	11.6	133	0.77
M(6)-3		1.74	0.67	4.14	7.87	431	0.83
M(6)-4		0.97	0.73	5.05	9.23	256	0.78
M(60)-1	60	1.48	0.69	8.31	90.2	4,710	0.58
M(60)-2		1.28	0.70	6.43	56.1	7,190	0.61
M(60)-3		3.44	0.72	7.63	56.7	2,020	0.59
M(90)-1	90	1.13	0.70	12.5	202	6,310	0.53
M(90)-2		2.79	0.69	6.99	44.9	155	0.61
M(120)-1	120	0.92	0.83	25.5	2,420	9,810	0.48
M(120)-2		0.48	0.92	21.2	127	129	0.48
M(120)-3		0.64	1.01	55.6	133	296	0.45
M(120)-4		0.85	0.96	46.3	146	218	0.45
M(120)-5		1.53	0.86	30.4	242	344	0.48
M(120)-6		1.77	0.85	32.5	558	632	0.47
M(120)-7		1.60	0.85	33.1	2,970	4,170	0.47
M(120)-8		2.72	0.78	12.2	61.1	351	0.54
M(120)-9		1.55	0.89	15.2	365	1,000	0.51
M(120)-10		1.19	0.72	11.9	484	4,250	0.53
M(120)-11		0.89	0.80	18.2	1,030	5,600	0.50
M(120)-12		0.71	0.81	25.9	4,560	9,170	0.48
M(120)-13		1.05	0.72	7.25	65.4	14,300	0.59
M(120)-14		1.31	0.71	10.2	234	42,900	0.54
M(120)-15		1.52	0.87	45.6	9,320	33,500	0.46
M(120)-16		1.29	0.92	21.8	94.3	865	0.49
M(120)-17		1.58	0.80	25.0	2,060	14,200	0.49
M(240)-1	240	0.89	0.87	39.7	5,050	9,350	0.46
M(240)-2		1.07	0.83	28.4	5,570	40,600	0.47

combination of gases could be predicted using the model calculation with previously measured permeance ratios.

Conversely, the experimental relationship between He/N_2 and He/SF_6 showed a somewhat scattering, as shown in Figure 9e. More specifically, the permeance ratio of He/SF_6 for corresponding He/N_2 ratios tended to be low compared with the theoretical values. This behavior could be attributed to the fact that the membranes might have a small number of large pores. The lower permeance ratio of He/SF_6 compared with the theoretical prediction indicates that SF_6 mainly permeated through the large pores such as defects or pinholes, while He and N_2 permeated through the micropores formed by the BTESE network pores.

Figure 10 shows the relationship of He/N_2 and H_2/N_2 permeance ratios for various types of microporous inorganic membranes including zeolite membranes,[23–26] and sol–gel,[22]

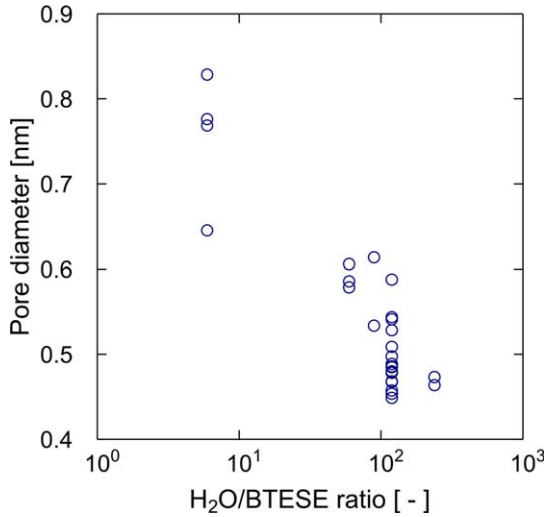

Figure 7. Relationship between estimated pore diameters and the H_2O/BTESE molar ratio for BTESE-derived membranes.

Pore sizes were estimated based on Eq. 14 using single gas permeance at 200°C. [Color figure can be viewed in the online issue, which is available at wileyonlinelibrary.com.]

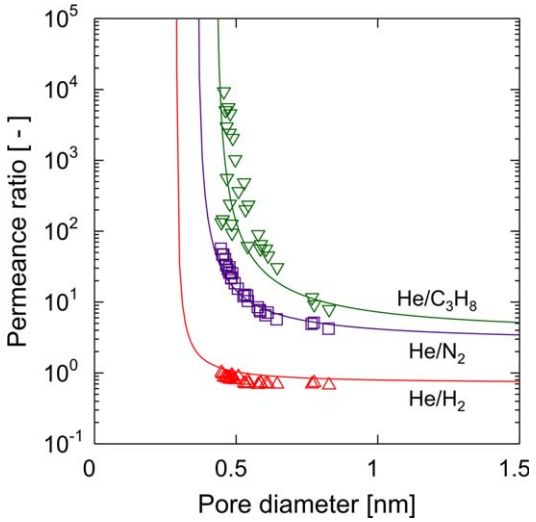

Figure 8. Relationship between the pore diameters and the permeance ratios of He/H_2, He/N_2, and He/C_3H_8 for BTESE-derived membranes.

Symbols: experimental; solid curves: calculated based on modified-GT model (Eq. 12). [Color figure can be viewed in the online issue, which is available at wileyonlinelibrary.com.]

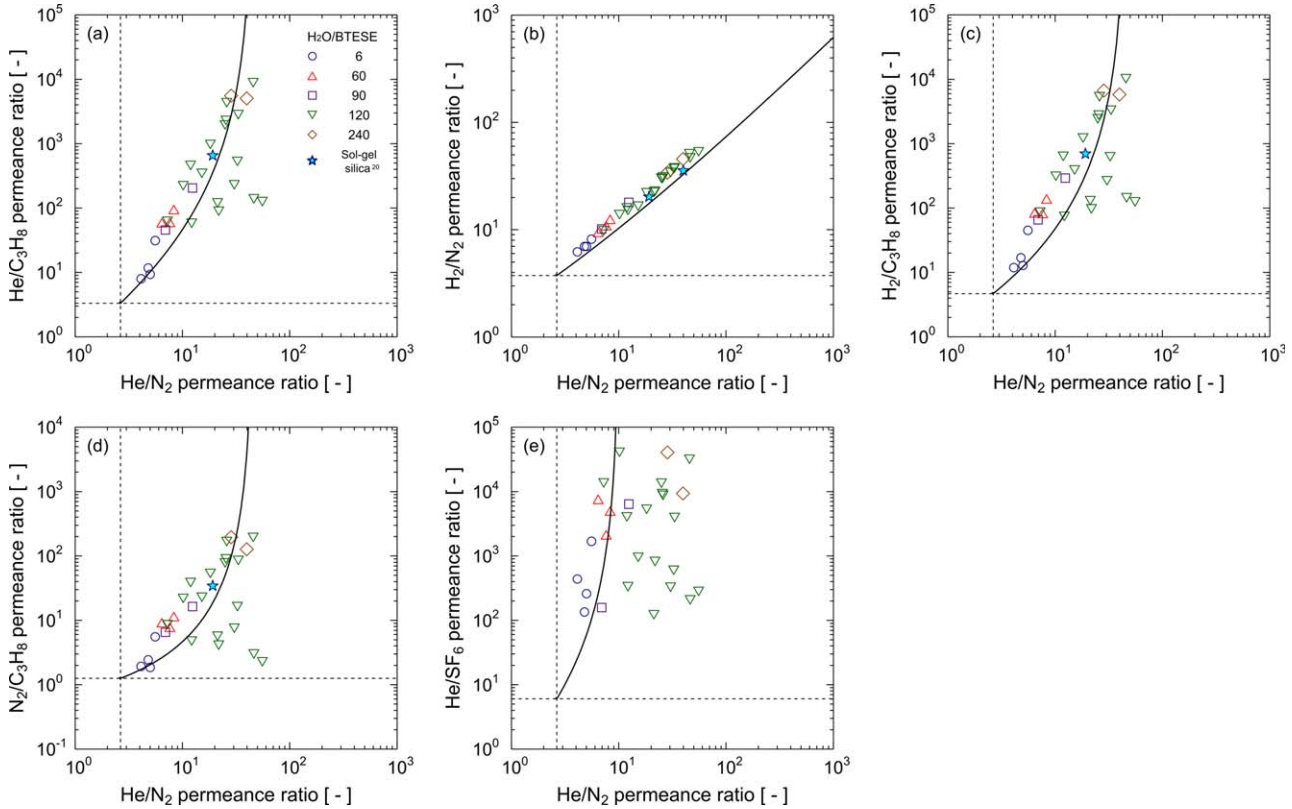

Figure 9. Permeance ratio relationships between He/N_2 and (a) He/C_3H_8, (b) H_2/N_2, (c) H_2/C_3H_8, (d) N_2/C_3H_8, and (e) He/SF_6 for BTESE-derived membranes and a sol–gel-derived silica membrane.[22]

Symbols: experimental; solid curves: calculated based on modified-GT model (Eq. 12). [Color figure can be viewed in the online issue, which is available at wileyonlinelibrary.com.]

CVD,[7,27,28] and plasma-enhanced CVD (PECVD)[29,30] derived silica membranes. The experimental results and the theoretical curve agreed well in a wide range of permeance ratios as high as 10^5. The results suggested that the modified-GT model can be used to describe the gas permeation mechanisms through the organosilica microporous membranes as well as through a wide variety of microporous inorganic membranes.

The modified-GT model represented in Eq. 8 can also be used to determine the theoretical permeance for BTESE membranes. Once the activation energy, $E_{P,i}$, is given, it is possible to predict the permeance and permeance ratios by introducing only one characteristic parameter, that is, the overall membrane structural parameter, $\varepsilon/\tau L$, with dimensions of inverse length.

The relationships between He or N_2 permeance and the He/N_2 permeance ratio at 200°C given by the modified-GT model are shown in Figure 11, in which the calculated results obtained from the three different values of the overall membrane structural parameter, $\varepsilon/\tau L$, were plotted. As BTESE membranes showed only a slight temperature dependence for He and N_2 (Figure 4), and because the gas permeation measurements were conducted at sufficiently high temperatures, the exponential term in Eq. 8 was assumed to be unity in this calculation. The He/N_2 permeance ratio decreased along with the increases of in He and N_2 permeance. As compared with the experimental results, the calculated results showed good agreement when using the overall membrane structural parameter value of $\varepsilon/\tau L = 3 \times 10^5\ m^{-1}$. If the values of ε and τ to be 0.2 and 2.0, respectively, which are the reasonable values for typical microporous membranes, the thickness of the BTESE layer, L, would be estimated to be approximately 300–350 nm. This was consistent with the SEM measurement results that we reported previously.[11]

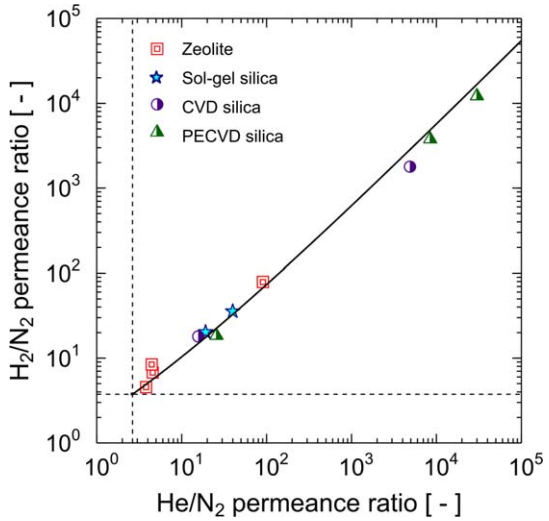

Figure 10. Permeance ratio relationship between He/N_2 and H_2/N_2 for microporous inorganic membranes including zeolite membranes[23–26] and silica membranes (Sol–gel,[22] CVD,[7,27,28] and PECVD[29,30]).

Symbols: experimental; solid curves: calculated based on modified-GT model (Eq. 12). [Color figure can be viewed in the online issue, which is available at wileyonlinelibrary.com.]

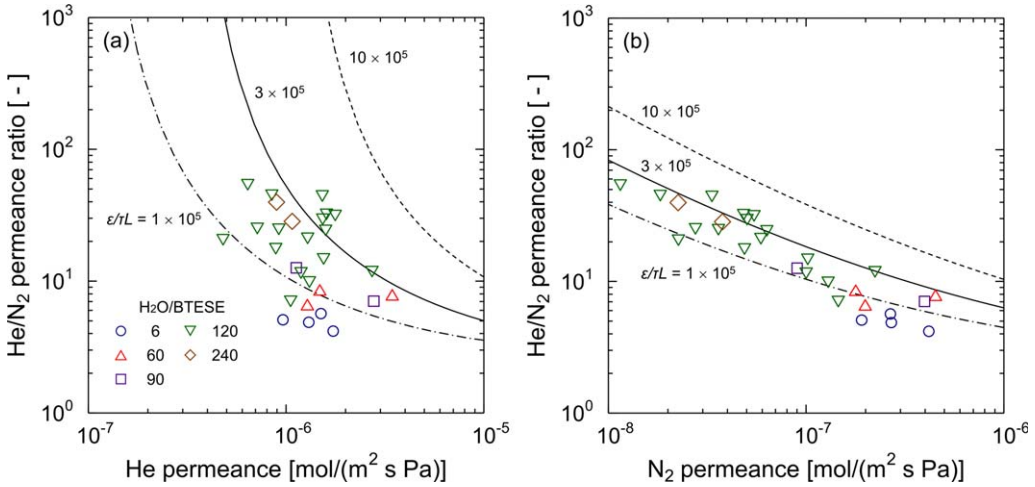

Figure 11. Relationship between He/N_2 selectivity and single gas permeances of (a) He and (b) N_2.

Symbols: experimental; curves: calculated based on modified-GT model (Eqs. 8 and 12) with the overall membrane structural parameter, $\varepsilon/\tau L = 1 \times 10^5$ (chain line), 3×10^5 (solid line), 10×10^5 m^{-1} (dashed line). [Color figure can be viewed in the online issue, which is available at wileyonlinelibrary.com.]

The relationships between N_2 permeance and the permeance ratios for various gas combinations given by the modified-GT model are shown in Figure 12. The overall membrane structural parameters, $\varepsilon/\tau L = 1 \times 10^5$, 3×10^5, and 10×10^5 m^{-1} were used for the theoretical calculations. Surprisingly, the permeance ratios for various gas

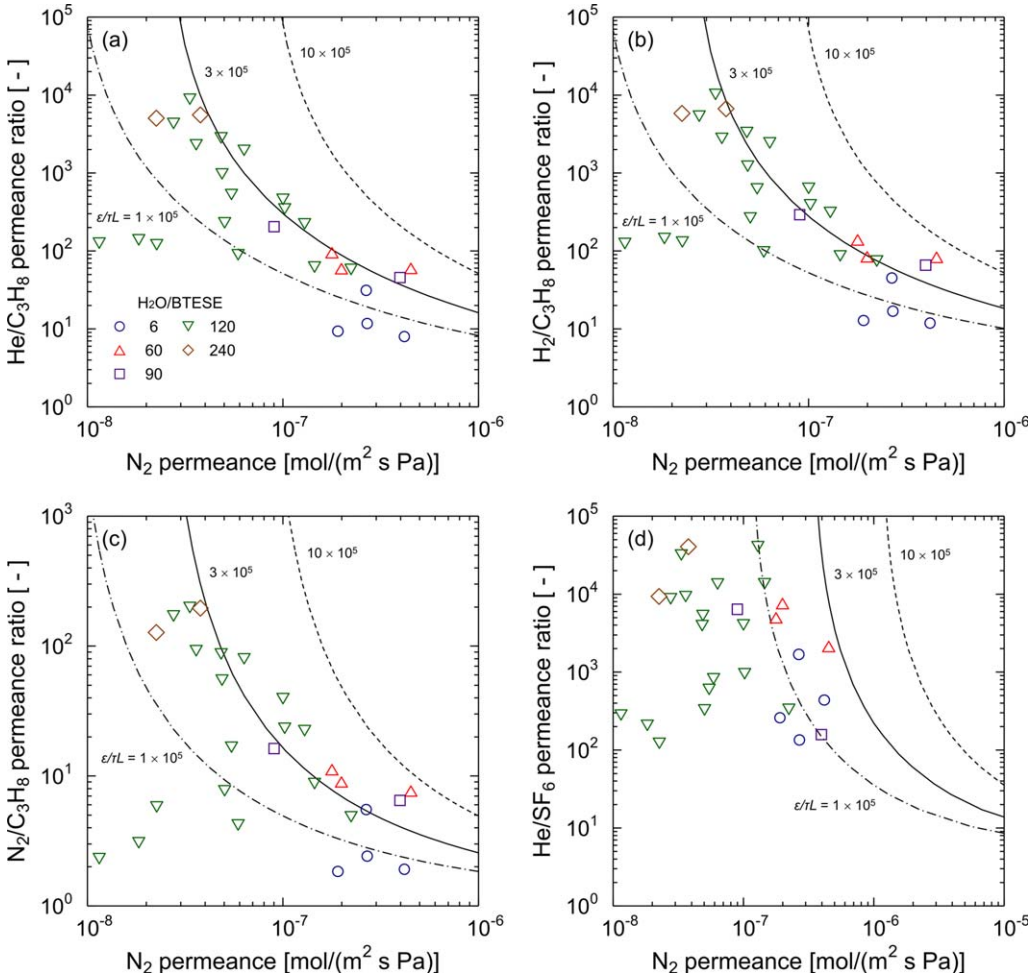

Figure 12. Gas permeation selectivity of BTESE-derived membranes for various gas combination [(a) He/C_3H_8, (b) H_2/C_3H_8, (c) N_2/C_3H_8, and (d) He/SF_6] as a function of N_2 permeance.

Symbols: experimental; curves: calculated based on modified-GT model (Eqs. 8 and 12) with the overall membrane structural parameter, $\varepsilon/\tau L = 1 \times 10^5$ (chain line), 3×10^5 (solid line), 10×10^5 m^{-1} (dashed line). [Color figure can be viewed in the online issue, which is available at wileyonlinelibrary.com.]

combinations, not only He/N_2 but also He/C_3H_8, H_2/C_3H_8, and N_2/C_3H_8, showed good agreement between the theoretical and the experimental results, even though the overall membrane structural parameter was at a constant value of $\varepsilon/\tau L = 3 \times 10^5$ m^{-1} for any combination of gases. Conversely, the experimental results of the He/SF_6 permeance ratio were much lower than the theoretical prediction curve. As SF_6 is one of the largest gas molecules and has extreme difficulty permeating through the BTESE networks, the reason for the large difference between the theoretical and the experimental results can again be attributed to the existence of a small number of large pores that SF_6 can permeate. Overall, as shown in Figures 11 and 12, using the modified-GT model, the theoretical calculation and experimental gas permeation data matched reasonably well. The results confirmed that the modified-GT model explained well the permeation properties through the BTESE-derived microporous membranes, and thus the model will be promising for its application to the theoretical prediction of gas permeation characteristics through a wide variety of microporous membranes.

Conclusions

The modified gas-translation (GT) model was applied to the characterization of sol–gel-derived organosilica membranes prepared using BTESE. The gas permeation characteristics of the BTESE-derived membranes were investigated as a function of the H_2O/BTESE ratio during the sol preparation step. The gas permeation selectivity of the BTESE-derived membranes was found to be controlled by the H_2O/BTESE molar ratio. The experimentally and theoretically obtained permeance and selectivity showed good agreement, which suggested that the modified-GT model had accurately described the transport phenomena in the BTESE-derived microporous membranes.

1. The gas permeation selectivity of BTESE-derived membranes tended to increase as the H_2O/BTESE molar ratio increased due to a high degree of initial hydrolysis leading to the formation of highly cross-linked sol. For example, at $H_2O/BTESE = 6$, the membranes showed a moderate selectivity with permeance ratios of 5.62 for He/N_2, and 30.8 for He/C_3H_8, while at $H_2O/BTESE = 240$, the membranes showed a pronounced selectivity of 39.2 for He/N_2, and 5,050 for He/C_3H_8. Moreover, the membrane derived from BTESE sol prepared at $H_2O/BTESE = 240$ showed a high hydrogen permeance of 1.02×10^{-6} mol/(m^2 s Pa) with high H_2/C_3H_8 and H_2/SF_6 selectivity of 5,810 and 10,700, respectively.

2. The activation energies for all types of gases increased as the H_2O/BTESE molar ratio increased, suggesting that the pore size of the BTESE-derived membrane was decreased with an increase in the H_2O/BTESE ratio. The permeation of He, H_2, and N_2 was governed by Knudsen diffusion when $H_2O/BTESE = 6$, while activated diffusion was dominant when $H_2O/BTESE = 120$ and 240. The permeation of C_3H_8 showed surface diffusion behavior due to a strong attractive interaction with the pore wall.

3. The pore sizes of BTESE membranes predicted by NKP analysis showed a tendency to decrease with an increase in the H_2O/BTESE ratio. It was suggested that changing the H_2O/BTESE ratio would control the size of the microporous network structures in the BTESE-derived membranes.

4. The trade-off curves of gas permeance and selectivity for BTESE-derived membranes were theoretically predicted based on the modified-GT model. The theoretical calculation results and experimental gas permeation data matched reasonably well. It was surprising that the permeance ratios for various gas combinations showed good agreement, even though the structural fitting parameter for model calculation was maintained at a constant value for all combinations of gases.

Acknowledgment

This work was supported by Core Research for Evolutional Science and Technology (CREST), the Japan Science and Technology Agency.

Notation

a = structural constant given by Eq. 16, m^{-3}
A_0 = physical cross-sectional area of pore, m^2
A_i = effective cross-sectional area of pore for ith component, m^2
A_m = membrane area, m^2
$d_{e,i}$ = effective diffusion length of ith component, m
d_i = kinetic diameter of ith component, m
d_p = pore diameter, m
d_S = kinetic diameter of standard gas, m
E_D = activation energy of diffusion for ith component, J/mol
$E_{P,i}$ = activation energy of permeation for ith component, J/mol
f_{NKP} = normalized Knudsen-based permeance, dimensionless
$-\Delta H_i$ = energy of interaction for ith component, J/mol
$k_{0,i}$ = permeation constant for ith component given by Eq. 10, dimensionless
L = membrane thickness, m
M_i = molecular weight of ith component, kg/mol
M_S = molecular weight of standard gas, kg/mol
N_p = the number of pores, dimensionless
P_i = permeance for ith component, mol/(m^2 s Pa)
P_S = permeance for standard gas, mol/(m^2 s Pa)
$P_{GT,i}$ = gas-translation model-based permeance for ith component, mol/(m^2 s Pa)
$P_{m\text{-}GT,i}$ = modified gas-translation model-based permeance for ith component, mol/(m^2 s Pa)
R = gas constant, J/(mol K)
T = absolute temperature, K

Greek letters

$\alpha_{i/j}$ = ideal selectivity for ith and jth components, dimensionless
ε = porosity, dimensionless
$\rho_{g,i}$ = geometrical probability for ith component, dimensionless
ρ_i = probability of diffusion for ith component, dimensionless
τ = tortuosity, dimensionless

Literature Cited

1. de Vos R, Verweij H. High-selectivity, high flux silica membranes for gas separation. *Science*. 1998;279:1710–1711.
2. Lu G, da Costa J, Duke M, Giessler S, Socolow R, Wiliams R, Kreutz T. Inorganic membranes for hydrogen production and purification: a critical review and perspective. *J Colloid Interface Sci*. 2007;314:589–603.
3. Yoshioka T, Tsuru T, Asaeda M. Molecular dynamics study of gas permeation through amorphous silica network and inter-particle pores on microporous silica membranes. *Mol Phys*. 2004;102:191–202.
4. Kanezashi M, Asaeda M. Hydrogen permeation characteristics and stability of Ni-doped silica membranes in steam at high temperature. *J Membr Sci*. 2006;271:86–93.
5. Battersby S, Tasaki T, Smart S, Ladewig B, Liu S, Duke M, Rudolph V, da Costa J. Performance of cobalt silica membranes in gas mixture separation. *J Membr Sci*. 2009;329:91–98.

6. Nomura M, Aida H, Gopalakrishnan S, Sugawara T, Nakao S, Yamazaki S, Inada T, Iwamoto Y. Steam stability of a silica membrane prepared by counter-diffusion chemical vapor deposition. *Desalination*. 2006;193:1–7.
7. Gu Y, Oyama ST. High molecular permeance in a poreless ceramic membrane. *Adv Mater*. 2007;19:1636–1640.
8. Raman NK, Brinker CJ. Organic "template" approach to molecular sieving silica membrane. *J Membr Sci*. 1995;105:273–279.
9. Castricum HL, Sah A, Kreiter R, Blank D, Vente JF, Ten Elshof JE. Hybrid ceramic nanosieves: stabilizing nanopores with organic links. *Chem Commun*. 2008:1103–1105.
10. Castricum HL, Sah A, Kreiter R, Blank D, Vente JF, Ten Elshof JE. Hydrothermally stable molecular separation membranes from organically linked silica. *J Mater Chem*. 2008;18:2150–2158.
11. Kanezashi M, Yada K, Yoshioka T, Tsuru T. Organic-inorganic hybrid silica membranes with controlled silica network size: preparation and gas permeation characteristics. *J Membr Sci*. 2010;348:310–318.
12. Niimi T, Nagasawa H, Kanezashi M, Yoshioka T, Ito K, Tsuru T. Preparation of BTESE-derived organosilica membranes for catalytic membrane reactors of methylcyclohexane dehydrogenation. *J Membr Sci*. 2014;455:375–383.
13. Devreux F, Boilot J, Chaput F. Sol-gel condensation of rapidly hydrolyzed silicon alkoxides: a joint 29Si NMR and small-angle x-ray scattering study. *Phys Rev A*. 1990;41:6901–6909.
14. Xiao J, Wei J. Diffusion mechanism of hydrocarbons in zeolites-I. *Theory*. *Chem Eng Sci*. 1992;47:1123–1141.
15. Shelekhin AB, Dixon AG, Ma YH. Theory of gas diffusion and permeation in inorganic molecular-sieve membranes. *AIChE J*. 1995;41:58–67.
16. Lee HR, Kanezashi M, Shimomura Y, Yoshioka T, Tsuru T. Evaluation and fabrication of pore-size-tuned silica membranes with tetraethoxydimethyl disiloxane for gas separation. *AIChE J*. 2011;57:2755–2765.
17. Yoshioka T, Kanezashi M, Tsuru T. Micropore size estimation on gas separation membranes: a study in experimental and molecular dynamics. *AIChE J*. 2013;59:2179–2194.
18. de Vos RM, Verweij H. Improved performance of silica membranes for gas separation. *J Membr Sci*. 1998;143:37–51.
19. Duke MC, Pas SJ, Hill AJ, Kin YS, da Costa JC. Exposing the molecular sieving architecture of amorphous silica using positron annihilation spectroscopy. *Adv Funct Mater*. 2008;18:3818–3826.
20. Yoshioka T, Nakanishi E, Tsuru T, Asaeda M. Experimental studies of gas permeation through microporous silica membranes. *AIChE J*. 2001;47:2052–2063.
21. Hacarlioglu P, Lee D, Gibbs GV, Oyama ST. Activation energies for permeation of He and H_2 through silica membranes: an ab initio calculation study. *J Membr Sci*. 2008;313:277–283.
22. Asaeda M, Yamasaki S. Separation of inorganic/organic gas mixtures by porous silica membranes. *Sep Purif Technol*. 2001;25:151–159.
23. Aoki K, Kusakabe K, Morooka S. Gas permeation properties of A-type zeolite membrane formed on porous substrate by hydrothermal synthesis. *J Membr Sci*. 1998;141:197–205.
24. Cui Y, Kita H, Okamoto K. Zeolite T membrane: preparation, characterization, pervaporation of water/organic liquid mixtures and acid stability. *J Membr Sci*. 2004;236:17–27.
25. Tomita T, Nakayama K, Sakai H. Gas separation characteristics of DDR type zeolite membrane. *Microporous Mesoporous Mater*. 2004;68:71–75.
26. Tang Z, Dong J, Nenoff T. Internal surface modification of MFI-type zeolite membranes for high selectivity and high flux for hydrogen. *Langmuir*. 2009;25:4848–4852.
27. Gopalakrishnan S, da Costa JD. Hydrogen gas mixture separation by CVD silica membrane. *J Membr Sci*. 2008;323:144–147.
28. Nagano T, Fujisaki S, Sato K, Hataya K, Iwamoto Y, Nomura M, Nakao S. Relationship between the mesoporous intermediate layer structure and the gas permeation property of an amorphous silica membrane synthesized by counter diffusion chemical vapor deposition. *J Am Ceram Soc*. 2008;91:71–76.
29. Nagasawa H, Shigemoto H, Kanezashi M, Yoshioka T, Tsuru T. Characterization and gas permeation properties of amorphous silica membranes prepared via plasma enhanced chemical vapor deposition. *J Membr Sci*. 2013;441:45–53.
30. Nagasawa H, Minamizawa T, Kanezashi M, Yoshioka T, Tsuru T. High-temperature stability of PECVD-derived organosilica membranes deposited on TiO_2 and SiO_2-ZrO_2 intermediate layers using HMDSO/Ar plasma. *Sep Purif Technol*. 2014;121:13–19.

Manuscript received Mar. 5, 2014, and revision received July 31, 2014.